Model of carbon nanofiber internal structure formation and instability of catalytic growth interface

I. A. Merkulov,[1,*] V. I. Merkulov,[2] A. V. Melechko,[2,3] K. L. Klein,[3,4] D. H. Lowndes,[2,3] and M. L. Simpson[2,3,4]
[1]*Ioffe Physico-Technical Institute, Russian Academy of Sciences, St.-Petersburg, Russia*
[2]*Materials Science and Technology Division, Oak Ridge National Laboratory, Oak Ridge, Tennessee 37830, USA*
[3]*Center for Nanophase Materials Sciences, Oak Ridge National Laboratory, Oak Ridge, Tennessee 37830, USA*
[4]*Materials Science and Engineering Department, University of Tennessee, Knoxville, Tennessee 37996, USA*
(Received 27 February 2007; published 17 July 2007)

It is well known that the internal structure determines the properties of carbon nanotubes and carbon nanofibers. However, a fundamental understanding of the processes that drive structure formation is missing, hindering the development of controlled synthesis strategies. Here we use theoretical calculations to explore the time evolution of the shape of the interface between the catalyst nanoparticle and its associated graphitic nanofiber at the initial stages of growth. This phenomenological description of the behavior of the catalyst nanoparticle-graphite interface constructed with model parameters provides new understanding of the mechanisms that control the internal structure of carbon nanofibers. We show that if the magnitude of the interface curvature exceeds a critical value κ_{crit}, the interface loses stability and a cavity forms in the center of the nanofiber.

DOI: 10.1103/PhysRevB.76.014109 PACS number(s): 61.46.−w, 61.48.+c

I. INTRODUCTION

The attractive physical and chemical properties of carbon nanotubes (CNTs) and carbon nanofibers (CNFs) enable a variety of applications such as electron field emission, gene delivery, composite materials, hydrogen and charge storage, scanning probes, and many others.[1–9] The ability to control the synthesis of carbon nanostructures is crucial for realization of these applications, and the internal structure of CNTs and CNFs is the most important aspect determining their properties. Unfortunately, control of their internal structure remains elusive due to a lack of a fundamental understanding of the processes that drive structure determination.

These nanostructures are composed of curved graphene sheets that are well approximated by cylindrical surfaces for nanotubes and conical surfaces for nanofibers. Over large distances the conical layers of nanofibers may lose their cylindrical symmetry; however, this symmetry can be restored or maintained by the presence of strong electric field during growth, which aligns the CNF along the direction of electric field.[10] In the case where the electric field is perpendicular to the substrate, the nanofibers are called vertically aligned carbon nanofibers (VACNFs), where the catalyst nanoparticle is located at the tip and serves as a conduit for converting carbon from the gas phase into graphene layers of a nanofiber.[1] An empty cavity is often observed at the nanofiber center[11] as in Fig. 1(a), or alternatively this cavity can be filled with either amorphous carbon[12] or catalyst material,[13] such as a nanowire shown in Fig. 1(b). With control over the internal structure, these nanostructures can be customized for specific applications. For example, a filled structure can be used for making magnetic nanowires,[13] while a continuous central cavity may be applied in nanofluidic devices.[14]

The internal structure of the nanofiber is a recorded history of the catalyst nanoparticle-graphite (CN-G) interface, which allows the comparison of the theoretical model to experimental data. Understanding the behavior of the CN-G interface requires the formulation of an appropriate model with parameters that can ultimately be mapped onto macroscopic experimental parameters.[15,16] In this work we construct a phenomenological description of the structural development of carbon nanofiber graphene layers at the initial stages of growth. Based on this model we analyze the stability of the evolving CN-G interface. The instability of the solution manifests physically as the transient loss of the CN-G interface and the formation of a cavity in the center of the nanofiber.

II. EXPERIMENTAL METHODS

The VACNF synthesis process is described in detail elsewhere[17] but will briefly be described here with several experimental examples of the phenomena discussed in this paper. Typical nanofibers grown by the catalytic plasma enhanced chemical vapor deposition (C-PECVD) method are shown in Fig. 1. These nanofibers were synthesized from a nickel catalyst thin film deposited onto a silicon substrate. Prior to growth, the thin film was pretreated with a brief etch in ammonia (NH_3) plasma (100 sccm, 10 Torr, 2 Amps) at 700 °C, which facilitated the formation of discrete nanoparticles from the continuous film. The nanofiber growth was initiated by the introduction of acetylene (C_2H_2) gas to the plasma at a rate of 80 sccm. In order to characterize the internal structure of the nanofibers, the fibers were removed from the substrate and transferred to TEM grids for transmission electron microscopy analysis (TEM, Hitachi HF-2000 and STEM HD-2000). Figures 1(c) and 1(d) show TEM images of carbon nanofibers that illustrate both continuous solutions and solutions with an internal orifice, where the graphitic layers become discontinuous. The edges of the orifice are indicated by the arrows in Fig. 1(c). This quasisteady state of discontinuous graphene layers appears only a certain time after growth initiation. At the initial moment of growth,

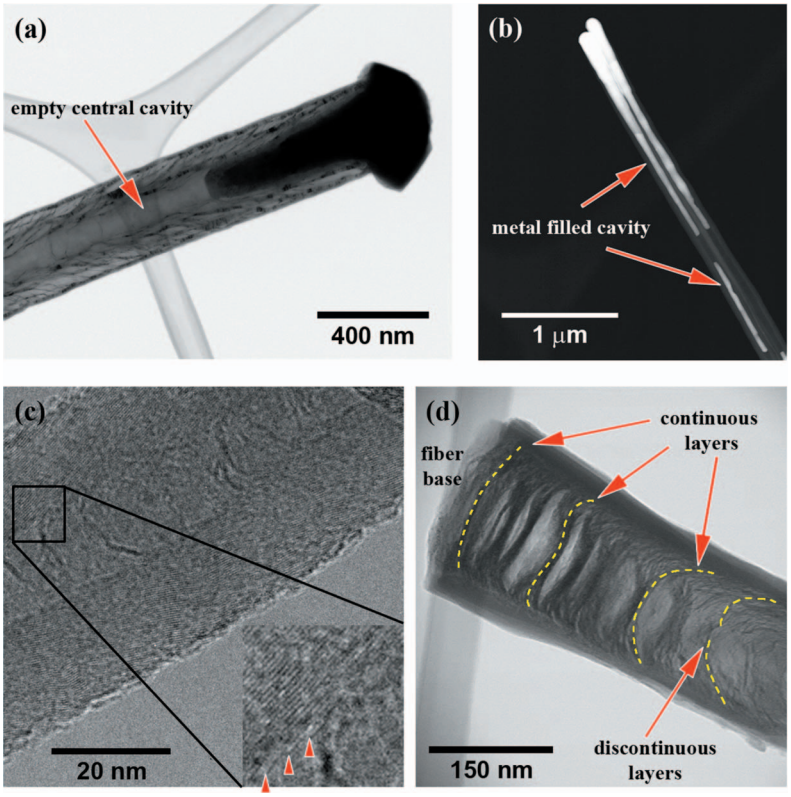

FIG. 1. (Color online) (a) Transmission electron microscopy image of a typical CNF with an empty central cavity. (b) Scanning transmission electron microscopy image of two carbon nanofibers in *z*-contrast mode. The white areas are where the nanofibers are filled with nickel. The nickel catalyst material has been sucked into the internal cavity during growth. (c) High-resolution transmission electron microscopy image of a nanofiber with central cavity. The inset shows where several graphitic planes terminate (see arrows) at the cavity. (d) Transmission electron microscopy image showing the profile of the initial stages of CNF growth. In this fiber the initially flat, continuous planes at the base of the fiber gradually curve upward. Eventually as the slope of the curves increase, the graphitic layers become discontinuous in the center of the nanofiber.

the catalyst nanoparticle is attached to the surface of a substrate, thus the first graphitic layers that appear between catalyst and substrate are flat or parallel to the substrate surface [see Fig. 1(d)]. The continuous planes at the base of the fiber gradually curve upward towards the catalyst particle. Eventually as the slope of the curves increase, the graphitic layers can become discontinuous in the center of the nanofiber.

III. MATHEMATICAL MODEL OF NANOFIBER GROWTH

While applicable to all carbon nanofiber growth, this work focuses on understanding the structure of VACNFs formed by C-PECVD.[6] VACNFs grow from a catalyst particle that begins on a flat substrate and is then pushed above the substrate, located at the tip of the nanofiber during growth. For the calculation of the change of shape of the interface between the catalyst and graphitic nanofiber we will use the kinematic approach suggested in Ref. 15. The approach used here is based on the phenomenological dependence of the magnitude of the velocity of the CN-G interface V_n on its curvature κ with precision up to the second order (κ^2),

$$V_n = V_{n,0} - \Gamma_1 \sum_{m=1,2} R_m^{-1} - \Gamma_2 \sum_{m=1,2} R_m^{-2} = \left(V_{n,0} + \frac{\Gamma_1^2}{2\Gamma_2} \right) - \sum_{m=1,2} \left(\frac{\Gamma_1}{2\Gamma_2} \vec{R}_m + \vec{n} \right)^2 \frac{\Gamma_2}{R_m^2}. \quad (1)$$

Here $V_{n,0}$ is the growth velocity of the flat interface and $\vec{R}_m$ are two radii of curvature of the interface. It is assumed that the vector radii point from the center of curvature toward the surface, i.e., curvatures of the growth front are negative for concave and positive for convex surfaces. The signs in (1) are chosen so that for positive values of phenomenological parameters (Γ_1, Γ_2) and the absence of additional limitations, the stable growth front remains flat. The values of $V_{n,0}, \Gamma_1, \Gamma_2$ are determined by growth conditions. In a general case they could vary for different points on the growth front, however accounting for these variations is beyond the scope of this work and in our calculations we will neglect this dependence.

The small bending toward a concave shape increases the growth rate, while bending toward convex decreases the growth rate. Large bending always slows growth down and, at a certain value of curvature, completely stops it.

Let us use dimensionless variables to express growth rates in units of $\Gamma_1^2/(4\Gamma_2)$, so that

$$v_n = V_n \frac{4\Gamma_2}{\Gamma_1^2}, \quad (2)$$

and with length in units of $2\Gamma_2/\Gamma_1$, Eq. (1) can be written as

$$v_n = (v_{n,0} + 2) - \sum_{m=1,2} (1 + \kappa_m)^2, \quad (3)$$

where $\kappa_m = \frac{2\Gamma_2}{\Gamma_1 R_m}$ are two dimensionless eigenvalues of the curvature tensor. It can be seen that the maximum normal growth rate,

$$v_{n,\max} = v_{n,0} + 2, \quad (4)$$

is reached at curvatures where $\kappa_1 = \kappa_2 = -1$. The curvature of the growth front ultimately determines the growth rate. With

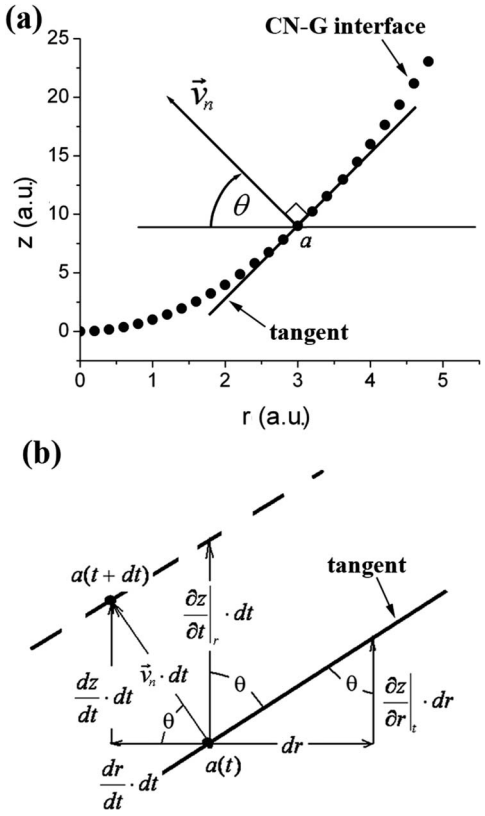

FIG. 2. (a) Schematic depicting one curve of the CN-G interface. Here the normal growth velocity, $\vec{v}_n$, is shown for point a on the curve. The angle θ is defined as the angle between the r axis and $\vec{v}_n$. (b) Detailed diagram of the translation during time dt of a section of the interface, showing the connection between the ordinary derivatives, partial derivatives, and the angle θ.

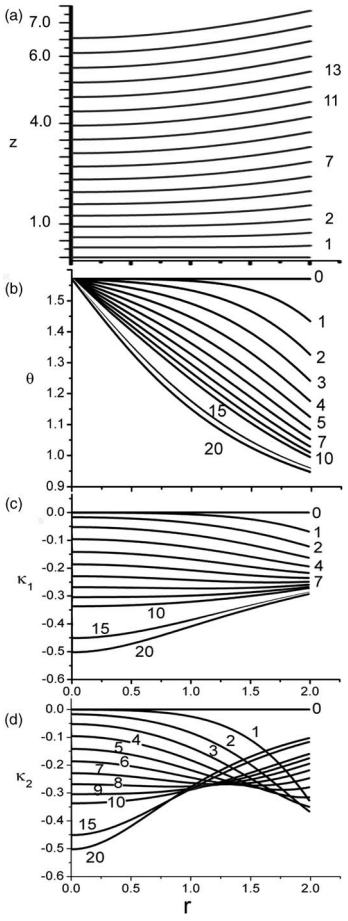

FIG. 3. (a) Change of shape of the interface at the initial stages of growth without central cavity formation (i.e., continuous solution). The parameter values for the numerical calculation are $v_{n,\max}=5$, $\Theta=0.3\pi$, $\tau=0.4$, and $r_{\max}=2$. The curve number n is related to dimensionless time by the formula $t(n)=n\cdot 0.1$. (b) Time evolution of the interface tilt angle at the initial stages of growth. The behavior of $\theta(r_{\max},t)$ varies according to Eq. (12), while the angle at the center remains constant, $\theta(0,t)\equiv\pi/2$. (c) Time evolution of the first curvature of the interface at the initial stages of growth. At $t\leqslant 2\tau$ (or $n\leqslant 8$), $|\kappa_1(r_{\max})|$ grows fast and saturates at ~ -0.3. (d) Time evolution of the second curvature at the initial stages of growth. At $t\ll\tau$ (or $n\ll 4$), $|\kappa_2(r_{\max})|$ increases rapidly, then maximizes and decreases, reaching a steady state of ~ -0.1.

increasing absolute value of negative curvature, the growth rate initially increases and then decreases after passing through the maximum. In this region $(\kappa_1,\kappa_2<-1)$ the growth rate of a more curved surface is less than a weakly curved one. As a result of this, the CN-G interface loses its stability, which is shown by the arguments below.

Here, as previously presented,[9] we will consider cylindrical nanofibers. In this case, the slope at every point on the CN-G interface at a given moment in time is defined by a single value of angle $\theta(z,r,t)$, where

$$\cot\theta = \left.\frac{\partial z}{\partial r}\right|_t. \tag{5}$$

The growth velocity $\vec{v}_n$ is directed perpendicularly from the CN-G interface, as shown in Fig. 2(a). The change in shape of the interface is defined by a system of differential equations [see Fig. 2(b) for clarification],

$$\frac{dr}{dt} = -v_n\cos\theta = -v_n\frac{\left.\frac{\partial z}{\partial r}\right|_t}{\sqrt{1+\left(\left.\frac{\partial z}{\partial r}\right|_t\right)^2}}, \tag{6}$$

$$\frac{dz}{dt} = v_n\sin\theta = v_n\frac{1}{\sqrt{1+\left(\left.\frac{\partial z}{\partial r}\right|_t\right)^2}}. \tag{7}$$

Note that if the CN-G interface shape is defined explicitly by $z(r,t)$, then

$$\left.\frac{\partial z}{\partial t}\right|_r = \frac{v_n}{\sin\theta} = \frac{dz/dt}{(\sin\theta)^2}. \tag{8}$$

The curvatures that appear in the relationship for growth velocity [Eq. (3)] are

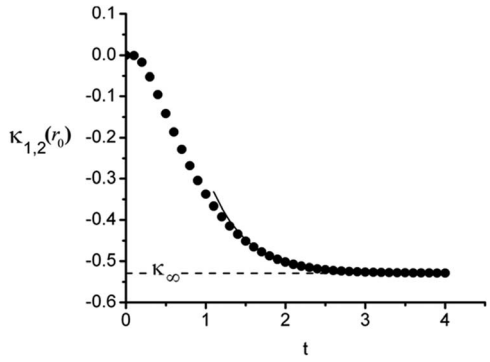

FIG. 4. Time dependence of curvature at the center of the interface. Dots are results from numerical calculation using Eqs. (3)–(12). The solid curve is an approximation of the asymptotic formula, Eq. (13), where $\kappa_\infty \approx -0.529$, $A \approx 3.58$, $\tau_\kappa \approx 0.413$.

$$\kappa_1 = -\frac{\cos\theta}{r} = -\frac{\left.\frac{\partial z}{\partial r}\right|_t}{r\sqrt{1+\left(\left.\frac{\partial z}{\partial r}\right|_t\right)^2}}, \tag{9}$$

$$\kappa_2 = -\frac{\partial}{\partial r}(\cos\theta) = -\left.\frac{\partial}{\partial r}\left(\frac{\left.\frac{\partial z}{\partial r}\right|_t}{\sqrt{1+\left(\left.\frac{\partial z}{\partial r}\right|_t\right)^2}}\right)\right|_t. \tag{10}$$

As we have already noted, for modest values of curvatures described by Eqs. (6) and (7), the deviations from the flat shape relax and disappear. For VACNFs, which grow from a catalyst particle located at their tip, the initial state of the CN-G interface is defined by the flat substrate. Hence, in order to describe the CN-G interface transformation from a flat interface into a conical one we must augment our model with a relation that would describe the action of physical mechanisms of bending. By itself, the bending of the growing graphite layers is energetically unfavorable. However, with such bending, the energy of the dangling bonds can be reduced at the periphery of the nanofiber, and so its free energy will be reduced as well. The forces that lead to bending, we believe, concentrate on the outer boundary of the CN-G interface, $r_{\max}$. Previously, it has been shown that bending occurs at the initial stages of growth,[18] although quantitative analysis of experimental results has not yet been performed. Here we consider that the rate at which the angle at the outer boundary, $\theta(r_{\max})$, changes proportionally to the deviation from its equilibrium value, Θ, is

$$\frac{d\theta(r_{\max})}{dt} = \frac{\Theta - \theta(r_{\max})}{\tau}. \tag{11}$$

Here τ is the characteristic relaxation time that depends on the nanofiber growth rate. Since at the initial moment of time $\theta(r_{\max}) = \pi/2$ (i.e., the interface is flat), $\theta(r_{\max})$, at any time, can be given by

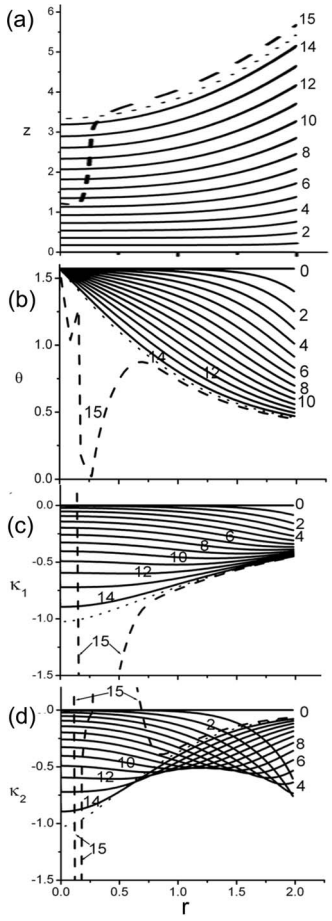

FIG. 5. (a) Change of the interface shape at the initial stages of growth for a nanofiber with central cavity formation (i.e., discontinuous solution). The parameters of the model are $v_{n,\max}=5$, $\Theta=0.1\pi$, $\tau=0.4$, and $r_{\max}=2$. The curve number is related to dimensionless time by the formula $t(n)=n0.06$. For $t>0.87$ (or $n\geqslant 15$, interface is indicated by the dotted line) an instability begins to develop in the central region of the interface. The growth rate in this region drops suddenly and can even become negative (see dashed line $n=15$). As a result, the deposition of carbon at the center of nanofiber is replaced by dissolution of the graphitic layers. With both positive (at $r_{\max}$) and negative (at r_0) interfacial velocities, the surface of catalyst detaches from the surface of graphite and the interface disappears. (b) Time evolution of the interface tilt angle at the initial stages of growth. The behavior of $\theta(r_{\max},t)$ is defined by Eq. (12), while $\theta(0,t)\equiv\pi/2$. The instability at $n\geqslant 15$ leads to sharp changes of $\theta(r,t)$ at the central region (see dashed line $n=15$). (c) Time evolution of the first curvature of the interface at the initial stages of growth. At $t\leqslant\tau$ (or $n\leqslant 7$), $|\kappa_1(r_{\max})|$ grows fast and reaches saturation. At the same time, the growth of the first curvature continues in the center of CNF so that $\kappa_1(r_0)$ becomes bigger than $\kappa_1(r_{\max})$. At $t\approx 0.87$ the dotted line $\kappa_1(r_0)<-1$ and the interface loses its stability. The curvature begins changing very fast and can even change its sign (see dashed line $n=15$). As a result, the interface disappears between catalyst and graphite in the central region of the fiber. (d) Time evolution of the second curvature at the initial growth stages. For $t\ll\tau$, $|\kappa_2(r_{\max})|$ grows fast, reaches a maximum and decays reaching steady state value $|\kappa_2(r_{\max},t\to\infty)| \ll |\kappa_1(r_{\max},t\to\infty)|$. At the center of the nanofiber $\kappa_1(r_0)=\kappa_2(r_0)$ and their behavior coincides. In the region of instability $\kappa_2(r)$ depends more strongly on the radius than $\kappa_1(r)$ (see dashed line $n=15$).

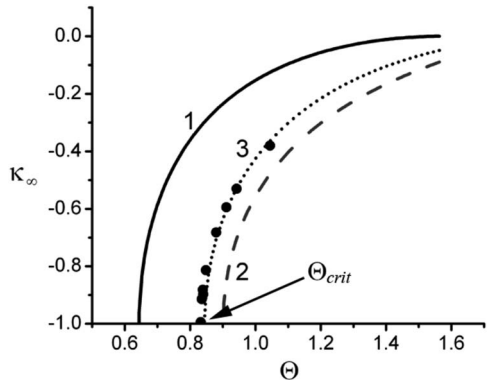

FIG. 6. Plot showing the dependence of the asymptotic value of the interface curvature at the center of the nanofiber κ_∞ on the equilibrium tilt angle Θ at the outer boundary. The calculation was performed using $v_{n,\max}=5$ and $r_{\max}=2$. The dotted points are obtained using formulas (3)–(12). The solid line 1 is calculated using asymptotic formula (15), valid for $r_{\max}\to\infty$. The dashed line 2 is obtained by neglecting the second curvature using formula (16). The dotted line 3 is obtained using Eq. (14), in which the second variable κ_2 is replaced by a constant value at $\Theta=0.3\pi$.

$$\theta(r_{\max},t)=\Theta+\left(\frac{\pi}{2}-\Theta\right)\exp\left(-\frac{t}{\tau}\right). \tag{12}$$

If $v_{n,\max}<v_{n,0}/\sin\Theta$, than in steady state the CN-G interface cannot exist at the center of the nanofiber. This is because the normal velocity at $r=0$ (r_0) would be smaller here than the velocity along the z axis $[\,\partial z/\partial t|_r$, Eq. (8)] at the periphery of the CN-G interface $(r_{\max})$. Figures 3 and 5 show examples of the transformation of interface with time, calculated according to formulas (3)–(12) for $v_{n,\max}=5$, $\Theta=\pi/3$, $\tau=0.4$, and $v_{n,\max}=5$, $\Theta=0.1\pi$, $\tau=0.4$, respectively. The number n of each curve is given for dimensionless time from growth initiation. For Fig. 3, $t(n)=0.1n$, and for Fig. 5, $t(n)=0.06n$.

In the first case $(\Theta=\pi/3)$, the interface remains stable for all points along the radius [Fig. 3(a)]. The tilt angle θ smoothly increases from center to periphery, with the angle at the center remaining constant at $\pi/2$ [Fig. 3(b)]. The first curvature κ_1 monotonically grows in time for all points of the interface and practically saturates for $n=20$ [Fig. 3(c)]. For small values of time $|\kappa_1(r_0)|<|\kappa_1(r_{\max})|$, while for large time $|\kappa_1(r_0)|>|\kappa_1(r_{\max})|$. The absolute value of the second curvature κ_2 at the outer surface of the nanofiber first increases fast and then falls to a steady state value where $|\kappa_2(r_{\max},t\gg\tau)|<|\kappa_1(r_{\max},t\gg\tau)|$ [Fig. 3(d)]. At the nanofiber center the magnitude of the second curvature grows monotonically. Also, due to cylindrical symmetry, $\kappa_1(r_0,t)\equiv\kappa_2(r_0,t)$. For large time, $\kappa_{1,2}(r_0,t)$ exponentially approaches its asymptotic value κ_∞ (Fig. 4),

$$\kappa_{1,2}(r_0,t)|_{t\to\infty}\approx\kappa_\infty+A\exp\{-t/\tau_k\}, \tag{13}$$

where $\tau_k\gg\tau$.

In the second case, $\Theta=0.1\pi$ for $t>0.87$, an instability occurs at the center of the nanofiber and a central cavity forms as seen in Fig. 5(a). The growth rate in this region drops suddenly and can even become negative. As a result, the deposition of carbon at the center of the nanofiber is replaced by dissolution of the graphitic layers. With both positive (at $r_{\max}$) and negative (at r_0) interfacial velocities, the surface of catalyst detaches from the surface of graphite and the interface disappears. In the regime of instability, the angle of the interface changes abruptly in the central region as shown by Fig. 5(b). As can be seen in Figs. 5(c) and 5(d) the instability develops in the region where $\kappa_{1,2}(r_0,t)<-1$. This is not just a coincidence.

Calculated results for the asymptotic value of curvature at the center of the interface κ_∞ are shown in Fig. 6 for various values of the equilibrium tilt angle Θ at the outer boundary. It appears that for the chosen parameters $(v_{n,\max}=5,\ r_{\max}=2)$ steady-state interface solutions exist only for $\Theta>\Theta_{\rm crit}\approx0.83$ and in the vicinity of this critical tilt angle $\kappa_\infty(\Theta)+1\propto\sqrt{\Theta-\Theta_{\rm crit}}$. In order to estimate the critical angle it is convenient to express κ_∞ in terms of curvatures and the angle at the outer surface,

$$\kappa_\infty=-1+\sqrt{\tfrac{1}{2}(v_{n,\max}-\{v_{n,\max}-[1+\kappa_1(r_{\max})]^2-[1+\kappa_2(r_{\max})]^2\}/\sin\Theta)}. \tag{14}$$

This formula is directly derived from the condition of equality of the interface shift velocity along the axis [Eq. (8)] for points at the center and outer boundary: $v_n(r_0)=v_n(r_{\max})/\sin\Theta$. $\kappa_1(r_{\max})$ is expressed in terms of Θ and $r_{\max}$ using Eq. (9) and does not require construction of the whole interface. However, calculation of $\kappa_2(r_{\max},\Theta)$, as well as direct calculation of κ_∞, without such construction is impossible. Obtaining a simple analytical expression for κ_∞ is possible if we assume a infinitesimal second curvature at the outer boundary. For large nanofiber radius, according to calculations in Ref. 15, the curvatures approach zero $[\lim_{r\to\infty}\kappa_{1,2}(r)=0]$ and Eq. (14) simplifies to

$$\kappa_\infty\approx-1+\sqrt{\tfrac{1}{2}[v_{n,\max}-(v_{n,\max}-2)/\sin\Theta]}. \tag{15}$$

The solid curve labeled 1 in Fig. 6 corresponds to the calculation of κ_∞ using formula (15). The error of the estimation of $\kappa_\infty(\Theta)$ for $v_{n,\max}=5$, $r_{\max}=2$ is around 25%. More precise estimation can be obtained if we recall $|\kappa_2(r_{\max},t\to\infty)|\ll|\kappa_1(r_{\max},t\to\infty)|$, and omit in (14) the second curvature only, substituting Eq. (9) for $\kappa_1(r_{\max})$,

$$\kappa_\infty \approx -1 + \sqrt{\frac{1}{2}\left\{ v_{n,\max} - \left[v_{n,\max} - \left(1 - \frac{\cos\Theta}{r_{\max}} \right)^2 - 1 \right] \Big/ \sin\Theta \right\}}. \tag{16}$$

The curve labeled 2 in Fig. 6 was obtained using this formula. For selected values of the parameters the error of such calculation is better than 10%.

To improve precision even more we can include κ_2 in (14) but omit its dependence on Θ. This estimation of the shape of the CN-G interface is found for one value of Θ. The result of the calculation of κ_2 for $\Theta=0.3\pi$ is given by curve 3. We see that the deviation of curve 3 from numerical calculations is not significant. In conclusion of this section we would like to emphasize that the calculated shape of the interface [Figs. 3(a) and 5(a)] reflects qualitative changes of the nanofiber structure during the initial stages of growth.[18] The tilting of graphene layers appears only in the vicinity of the outer boundary of the nanofiber [curves 1–3 of Figs. 3(a) and 5(a)]. In time the whole interface bends [curves 4–10 of Figs. 3(a) and 5(a)]. For sufficiently large values of Θ, where $\Theta > \Theta_{\text{crit}}(r_{\max}, v_{n,\max})$, the interface loses its stability in the central part of the nanofiber. In the following section we will demonstrate that the interface under non-steady-state conditions loses stability when curvatures $\kappa_{1,2}(r_0,t) < -1$.

IV. SHAPE STABILITY OF CURVED CN-G INTERFACE

The process of creation of the central cavity in the nanofiber can be split into two stages. In the first stage, the parameters of the system are far from critical and changes occur slowly on large time scale. Qualitatively, the behavior of the system at this stage does not contain surprises while it does include many possible mechanisms responsible for such behavior. We are referring here to the case of bending of the interface from flat, zero value of curvature, to its critical value $\kappa_{\text{crit}}=-1$, under the influence of forces acting at its outer boundary.

At the second stage large sharp sudden changes of interface shape occur. Here it is only imperative that $\kappa_{1,2}(r_0,t) < \kappa_{\text{crit}}=-1$, while how this curvature value was approached is inconsequential. Let us consider in zero approximation a piece of interface with curvature $\tilde{\kappa}$, that is near critical. In the corresponding cross section it has a shape of an arc with radius $\tilde{R}=\tilde{\kappa}^{-1}$ ($z \approx z_0 + \tilde{R}\cos\vartheta$, $x \approx x_0 + \tilde{R}\sin\vartheta$). Let us analyze how small deviations of this shape from the circle $\delta R(\vartheta) = R(\vartheta) - \tilde{R} \ll \tilde{R}$ evolve. Let us consider that these fluctuations are sufficiently slow such that the interface curvature is given by the following formula:

$$\kappa = \left(R + \frac{d^2R}{d\vartheta^2} \right)^{-1} \approx R^{-1}. \tag{17}$$

In this approximation

$$\frac{d\delta R}{dt} \approx -2(1+\tilde{\kappa})\tilde{\kappa}^2 \delta R. \tag{18}$$

That is

$$\delta R(\theta,t) = \delta R(\theta,0)\exp\left(-2\int_0^t (1+\tilde{\kappa})\tilde{\kappa}^2 dt \right). \tag{19}$$

Hence, while $\tilde{\kappa}(t) > \kappa_{\text{crit}}=-1$, the shape fluctuations decay exponentially. At the same time for large negative curvature $\tilde{\kappa}(t) < \kappa_{\text{crit}}$, fluctuations begin to grow exponentially and the interface loses its stability. After certain time the curvature becomes so large that the approximation itself no longer makes sense. Note that the condition $\kappa < \kappa_{\text{crit}}$ does not necessarily have to be realized in the nanofiber center. For instance, at the initial stage of growth the maximum bending occurs at the outer boundary and curvatures there could exceed the critical value. The maximum absolute value of the curvature in the nanofiber center is achieved only after sufficient time passes from the beginning of growth [Fig. 3(c) and 5(c)]. The observed experimental changes of the shape are in agreement with the idea that the interface is lost near the edges of the nanofiber during the initial stages of growth [second dashed line of Fig. 1(d)].

V. PHENOMENOLOGICAL MODEL IN RELATION TO PHYSICAL GROWTH PROCESS

After opening of the central orifice, the development of the interface between catalyst and nanofiber loses stability and depends on new details pertaining to the catalyst behavior of "exuding" carbon. Depending on experimental conditions the catalyst can partially get sucked into this central cavity [Fig. 1(b)] or form a semifree surface above this cavity. It seems that the rate of graphite deposition on this surface where $v_{n,\max} < v_{n,0}/\sin\Theta$ is not sufficiently large for formation of continuous graphite monolith from the nanofiber center to the outer radius (namely, this physical circumstance is reflected by a mathematical account of the absence of the solution for the interface inside the central region).

The low average density of graphite in the central region can correspond to two possible filling regimes. In the first case, the growth proceeds monotonically and the central region is filled with amorphous carbon. This is commonly seen with herringbone structure fibers. In the second case, graphite layers alternate with cavities. These carbon layers span the cavity like "cross struts" in bamboolike nanofibers. The cross struts are often flat or only slightly curved and form during a jumplike motion of the interface.[19]

For post-critical description of the interface our model must be augmented with new details. The differences between herringbone and bamboolike structures are not limited

to merely qualitative differences in length l_h and frequency τ_h^{-1} of interface jumps. The important parameter here is the ratio of the characteristic length, $v_t\tau_h$, of graphite growth in time between jumps compared to the radius of the central orifice $r_{\min}$. (Let us remember that all calculations presented above were conducted with the approximation $v_t \gg v_n$, where v_t is the tangential growth rate in the plane of the graphite sheet.[15]) From general consideration it is natural to assume that structures where $v_t\tau_h \gg r_{\min}$ are related to bamboolike type, while structures where $v_t\tau_h \ll r_{\min}$ are related to herringbone. However, the precise criteria of such a division requires construction of a physical model of filling the nanofiber central cavity, accounting not only for the process of deposition of carbon but also stresses that occur in the graphene layers as well as the plasticity of a catalyst material, stress distributions in it, etc.

Let us now discuss the processes that define two main parameters of the phenomenological model under consideration: maximum normal velocity $v_{n,\max}$ and equilibrium tilt angle Θ of graphite layers. The growth of a nanofiber is a result of a multistep chemical reaction in the process of which carbon is believed to dissolve in the catalyst and then segregates at the growth interface from a supersaturated solution. The outer surface of the catalyst remains uncovered by carbon layers in PECVD systems due to etching plasma, thereby preventing catalyst deactivation. The transport of carbon from the outer surface is usually linked with its bulk diffusion,[20] however some authors[21] credit the surface diffusion pathway. In order to vary the growth rate it is necessary to change the degree of saturation of the carbon solution in the catalyst[22] or reduce the supply of gaseous precursor.

The main factors defining the tilt angle Θ undoubtedly are forces of surface tension. Nolan *et al.*[23] connect it to the density of dangling carbon bonds at the outer boundary of the nanofiber. The energy of the dangling bonds is very large and they are neutralized by hydrogen captured from plasma directly. Thus, in equilibrium conditions, the higher concentration of atomic hydrogen available should correspond to a larger tilt angle. In Ref. 23 a formula is derived that relates hydrogen concentration and tilt angle. One of the basic phenomenological parameters of this theory is the outer radius of the nanofiber, responsible for the ratio of surface and bulk energies. The value of this radius is determined by the size of the catalyst particle, which in turn is determined by the effects of surface tension during the annealing step. Hence in the framework of the theory developed in Ref. 23 the angle of the graphene layers in the nanofiber indirectly depends on the surface tension of the catalyst. In the work presented here we discuss surface tension as if the catalyst particle is in a liquidlike state. This is justified for nanoparticles that are capable of changing their shape due to mass transport along the surface for temperatures smaller than the melting temperature of the bulk material.[24,25] It is necessary to note, however, that curving of the bottom of the catalyst particle leads to a lowering of its surface energy at least during detachment from the substrate. Further improvement of the model[23] must probably include accounting for the change of surface energy of a catalyst. In any case, the angle that is introduced to this phenomenological model should be determined from experiment or a more detailed theoretical model.

VI. CONCLUSIONS

In this paper we present a theoretical analysis of the shape of the interface between catalyst nanoparticle and growing carbon nanofiber in the initial stages of nanofiber growth. The phenomenological description is formulated with a curvature dependent propagation velocity of the growth interface. The main parameters of this theory are maximum normal catalyst nanoparticle–graphite interface velocity $v_{n,\max}$, the tilt angle Θ at the outer boundary of the CN-G interface, and nanofiber radius $r_{\max}$. The model developed here describes the main qualitative behavior of the interface as well as different peculiarities of CN-G interface behavior. In particular, it has been shown that there is a critical value of the interface curvature κ, such that for $\kappa < \kappa_{\text{crit}} = -1$ the interface loses its stability, resulting in a solution corresponding to the formation of a cavity inside the carbon nanofiber. This phenomenological description of the behavior of CN-G interface with model parameters, which ultimately can be mapped onto macroscopic experimental parameters, is a step toward understanding the mechanisms that control the internal structure of a carbon nanofiber.

ACKNOWLEDGMENTS

This work was sponsored by the Division of Materials Sciences and Engineering of the DOE Office of Science [for three of the authors (M.L.S., A.V.M., and I.A.M.)]. This work was performed at Oak Ridge National Laboratory, managed by UT-Battelle, LLC, for the US DOE under Contract No. DE-AC05-00OR22725. A portion of this research was conducted at the Center for Nanophase Materials Sciences, which is sponsored at Oak Ridge National Laboratory by the Division of Scientific User Facilities, US Department of Energy. The authors would like to thank David Keffer for fruitful discussions.

*Also at Materials Science and Technology Division, Oak Ridge National Laboratory, Oak Ridge, Tennessee 37830.

[1] R. T. K. Baker, Carbon **27**, 315 (1989).
[2] N. M. Rodriguez, J. Mater. Res. **8**, 3233 (1993).
[3] N. M. Rodriguez, A. Chambers, and R. T. K. Baker, Langmuir **11**, 3862 (1995).
[4] K. P. De Jong and J. W. Geus, Catal. Rev. - Sci. Eng. **42**, 481 (2000).
[5] H. J. Dai, Surf. Sci. **500**, 218 (2002).
[6] A. V. Melechko *et al.*, J. Appl. Phys. **97**, 041301 (2005).
[7] M. A. Guillorn *et al.*, J. Vac. Sci. Technol. B **22**, 35 (2004).
[8] T. E. McKnight *et al.*, Nano Lett. **4**, 1213 (2004).
[9] Q. Ye *et al.*, Nano Lett. **4**, 1301 (2004).
[10] V. I. Merkulov *et al.*, Appl. Phys. Lett. **79**, 2970 (2001).

[11] M. Endo *et al.*, Carbon **41**, 1941 (2003).
[12] R. T. K. Baker *et al.*, J. Catal. **26**, 51 (1972).
[13] A. L. Elias *et al.*, Nano Lett. **5**, 467 (2005).
[14] B. J. Hinds *et al.*, Science **303**, 62 (2004).
[15] I. A. Merkulov, A. V. Meleshko, J. C. Wells, H. Cui, V. I. Merkulov, M. L. Simpson, and D. H. Lowndes, Phys. Rev. B **72**, 045409 (2005).
[16] M. Chhowalla *et al.*, J. Appl. Phys. **90**, 5308 (2001).
[17] V. I. Merkulov *et al.*, J. Phys. Chem. B **106**, 10570 (2002).
[18] H. Cui *et al.*, Appl. Phys. Lett. **84**, 4077 (2004).
[19] C. J. Lee and J. Park, Appl. Phys. Lett. **77**, 3397 (2000).
[20] R. T. K. Baker *et al.*, J. Catal. **30**, 86 (1973).
[21] L. E. Jensen *et al.*, Nano Lett. **4**, 1961 (2004).
[22] J. W. Snoeck, G. F. Froment, and M. Fowles, J. Catal. **169**, 240 (1997).
[23] P. E. Nolan, D. C. Lynch, and A. H. Cutler, J. Phys. Chem. B **102**, 4165 (1998).
[24] U. Tartaglino *et al.*, Phys. Rep. **411**, 291 (2005).
[25] K. J. Strandburg, Rev. Mod. Phys. **60**, 161 (1988).